Nuclear Materials and Energy 12 (2017) 1248–1252

Contents lists available at ScienceDirect

Nuclear Materials and Energy

journal homepage: www.elsevier.com/locate/nme

Initial studies of plasma facing component surface conditioning in the national spherical tokamak experiment upgrade with the materials analysis particle probe

F. Bedoya[a,*], J.P. Allain[a], R. Kaita[b], C.H. Skinner[b], B.E. Koel[c], F. Scotti[d]

[a] Department of Nuclear, Plasma and Radiological Engineering, University of Illinois, Urbana, IL 61801, United States
[b] Princeton Plasma Physics Laboratory, Princeton, NJ 08543, United States
[c] Department of Chemical and Biological Engineering, Princeton University, Princeton, NJ 08540, United States
[d] Lawrence Livermore National Laboratory, Livermore, CA 94550, United States

ARTICLE INFO

Article history:
Received 14 July 2016
Revised 14 February 2017
Accepted 29 March 2017
Available online 6 April 2017

Keywords:
XPS
Boronized graphite
Conditioning
Plasma facing components
NSTX-U

ABSTRACT

An innovative PFC diagnostic, the Materials Analysis Particle Probe (MAPP) was used to study the chemistry of Plasma Facing Components (PFCs) in the National Spherical Tokamak Experiment Upgrade (NSTX-U). NSTX-U used boronization as conditioning strategy during the 2015–2016 experimental campaign. Deposition with ~9.1 g of deuterated tri-methyl boron (d-TMB) in a helium glow discharge resulted in coatings with an equivalent thickness of 7.0 nm at the lower outer divertor region. MAPP was used to capture for the first time the *in-vacuo* evolution of the chemical state of ATJ graphite PFCs after boronization and plasma exposure via X-ray Photoelectron Spectroscopy (XPS) on a day-to-day basis. The XPS data shows the formation of B_4C on the PFCs surface during boronization. We observed the gradual increase of the B_2O_3 fraction in the coatings with plasma exposures. In contrast, we measured the formation of non-stoichiometric oxides when the samples were only exposed to residual gases and an argon vent. MAPP data revealed erosion and oxidation of deposited boron coatings over the course of tens of shots (a time resolution improved several orders-of-magnitude compared to post-campaign PFC characterization) that is correlated with the transitory nature of plasma performance enhancement with boron conditioning.

Published by Elsevier Ltd.
This is an open access article under the CC BY-NC-ND license.
(http://creativecommons.org/licenses/by-nc-nd/4.0/)

1. Introduction

Conditioning of Plasma Facing Components (PFCs) has proven to have dramatic effects in plasma performance in both tokamaks and stellarators [1]. The National Spherical Torus eXperiment, NSTX, has recently undergone a major upgrade to NSTX-U in order to develop the physics basis for a ST-based Fusion Nuclear Science Facility (FNSF) [2]. One of the major mission elements of NSTX-U is to understand and develop novel solutions to the plasma-material interface. An understanding of the key chemical processes that govern materials mixing and surface response to implanted impurities is crucial to establish sustainable operational regimes under reactor-relevant conditions. Many studies have documented the improvements associated with glow discharges, vessel bake outs and deposition of coatings on PFCs [1], however a clear understanding of the changes in the surface chemistry correlated in the time scale of plasma behavior (e.g. a few plasma shots) is still critically missing [3,4].

The Materials Analysis Particle Probe (MAPP) is an *in-vacuo* surface chemistry characterization facility, designed to analyze samples exposed to tokamak plasmas in-between plasma shots, daily or weekly. The measurements can be done at the characteristic depth of chemical interactions of implanted and recycled edge-plasma particles [5]. In contrast with previous in situ surface characterization facilities, MAPP provides a time resolution on the same scale as the modification induced on the surface by the plasma exposures. Furthermore, MAPP carries four different samples that can be replaced independently thus characterizing PFCs with different conditioning and plasma exposure histories. Additionally, the samples, located in four different positions provide a picture of the spatial dependence of the chemistry in the area surrounding the holder's location. These, added to the highly surface-sensitive/non-destructive character of MAPP's techniques make it possible to draw a better correlation back to plasma performance than previously achievable [6–9]. MAPP was integrated to the Lithium

* Corresponding author.
E-mail address: bedoya2@illinois.edu (F. Bedoya).

http://dx.doi.org/10.1016/j.nme.2017.03.035
2352-1791/Published by Elsevier Ltd. This is an open access article under the CC BY-NC-ND license. (http://creativecommons.org/licenses/by-nc-nd/4.0/)

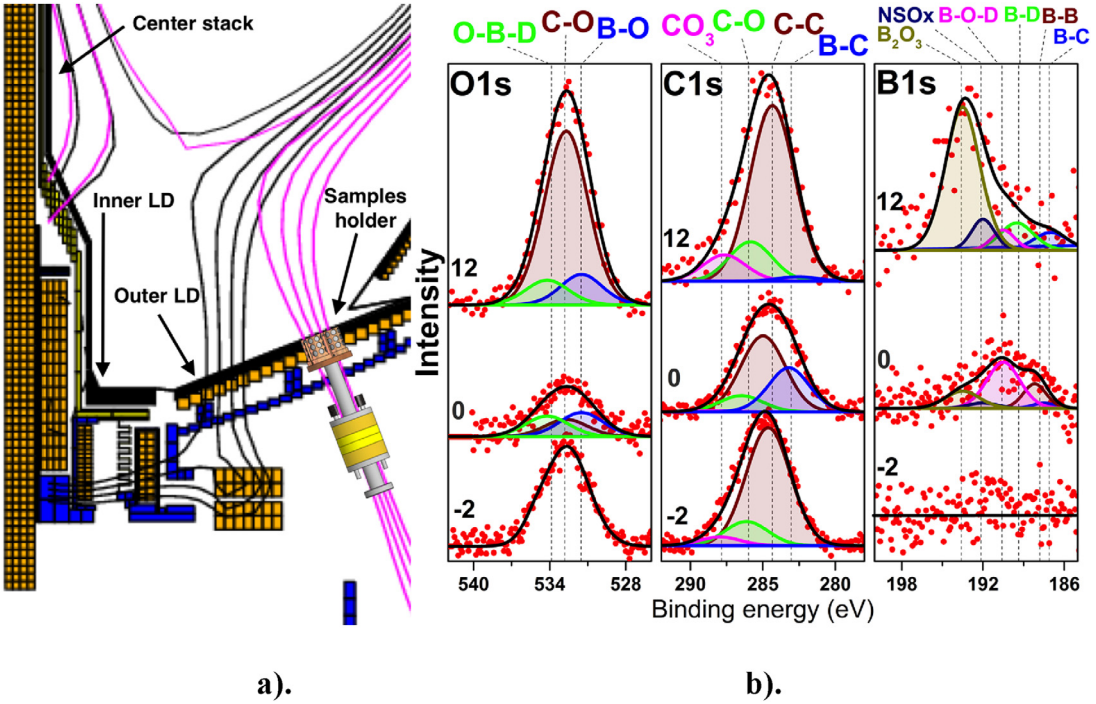

Fig. 1. a). Schematic representation of MAPP's sample holder in position flush with the tiles of the lower divertor (LD) of the tokamak, low and high δ discharges are overlapped for illustration purposes, b).O1s, C1s and B1s XPS region scans of the ATJ graphite sample; virgin (−2), boronized (0) and boronized following twelve days of plasma operations (12).

Tokamak Experiment (LTX) for proof-of-concept testing [10] and was later installed in NSTX-U for the 2015–2016 experimental run. NSTX-U used boronization for conditioning of its graphite PFCs during the campaign and MAPP was used to analyze an ATJ graphite sample exposed with the PFC surfaces in the tokamak.

A conditioning procedure frequently applied to vacuum vessels is to coat their inner surface with thin layers of different materials [1]. One material commonly used as a conditioning coating in tokamak machines is boron [11]. Boronizations are usually applied via Plasma Vapor Deposition (PVD) with a mixture of a buffer gas and boron carrying molecules [11]. This kind of conditioning improved machine performance reducing the amount of impurities in the plasma that in turn gave operational advantages such as the reduction of the H-mode power threshold. These improvements are generally attributed to the formation of oxides from reactions with residual gasses in the vacuum that reduce the sputtering yield of boronized graphite [12]. Multiple studies have been focused on the chemistry of boronized surfaces and in particular on boronized graphite. However, those studies have been performed in samples exposed to plasmas over a whole campaign with a variety of conditions, thus hindering the task of correlating plasma performance with the surface chemistry [13–17]. This work reports for the first time the chemical evolution of boronized graphite exposed to D^+ tokamak plasma discharges on a day-to-day basis. In particular, this includes; firstly, the characterization of the composition of the coatings resulting after boronization. Secondly, a characterization of the oxide compounds formed with plasma exposure and their comparison with those formed during exposure to residual gases. And thirdly, for the first time, a detailed documentation of the chemical changes occurring in the time scale of tens of plasma discharges (compared with hundreds to thousands) [17–22].

2. Materials and methods

NSTX-U is a spherical tokamak designed to operate with a maximum value of $I_P \leq 2$MA and $B_T \leq$ 1T [2,23]. The machine can operate in single and double null diverted configurations. Both divertors, as well as the surfaces of the first wall are made of ATJ and POCO graphite. In the 2015–2016 experimental run, NSTX-U used boronization to condition its PFC surfaces. Boron was deposited via plasma chemical vapor deposition (PCVD) with a DC discharge that used a gas mixture of 95% He and 5% deuterated Trimethyl Boron (d-TMB). The thickness of the resulting coatings was measured to be 7 nm in the lower divertor for boronization with 9.1 g d-TMB. Details on the boronization procedures in NSTX-U can be found in ref. [24]. Although boronization allowed plasma operations with low impurity levels and as a consequence better plasma performance, those effects were in general temporary and faded away in the course of a week [25].

MAPP's samples are inserted about 4 mm above the lower divertor tiles at a radius of 107.5 cm from the axis of the tokamak [26] (Fig. 1a). The MAPP probe has an innovative design that can hold up to four samples. One ATJ sample and one Au sample were used in this analysis. Baseline XPS spectra were collected before boronization and plasma exposure. Subsequent measurements consisted of withdrawing the MAPP probe head just after boronization for XPS characterization (usually 30 min after boronization was finished) to obtain the post-boronization data sets. After this, the MAPP probe head was again inserted about 4 mm above with the divertor tiles for plasma operations. Additional data sets were collected after a day of plasma operations. This procedure was repeated for additional boronization. Each XPS data set included regional scans for the B1s, C1s and O1s peaks and a survey scan. Binding energy calibration was performed using the $4f_{5/2}$ peak (88 eV) of the Au sample. The raw XPS data was fitted using CASAXPS software (v 2.3).

3. Results

Fig. 1b shows a comparison of three XPS region scans between an untreated ATJ graphite sample (labeled "−2"), the same sample immediately after boronization ("0") and after 12 days of plasma exposures ("12"). In the untreated sample, one peak is fitted in the O1s region at 532.7 eV and it is assigned to C–O bonds. In the C1s

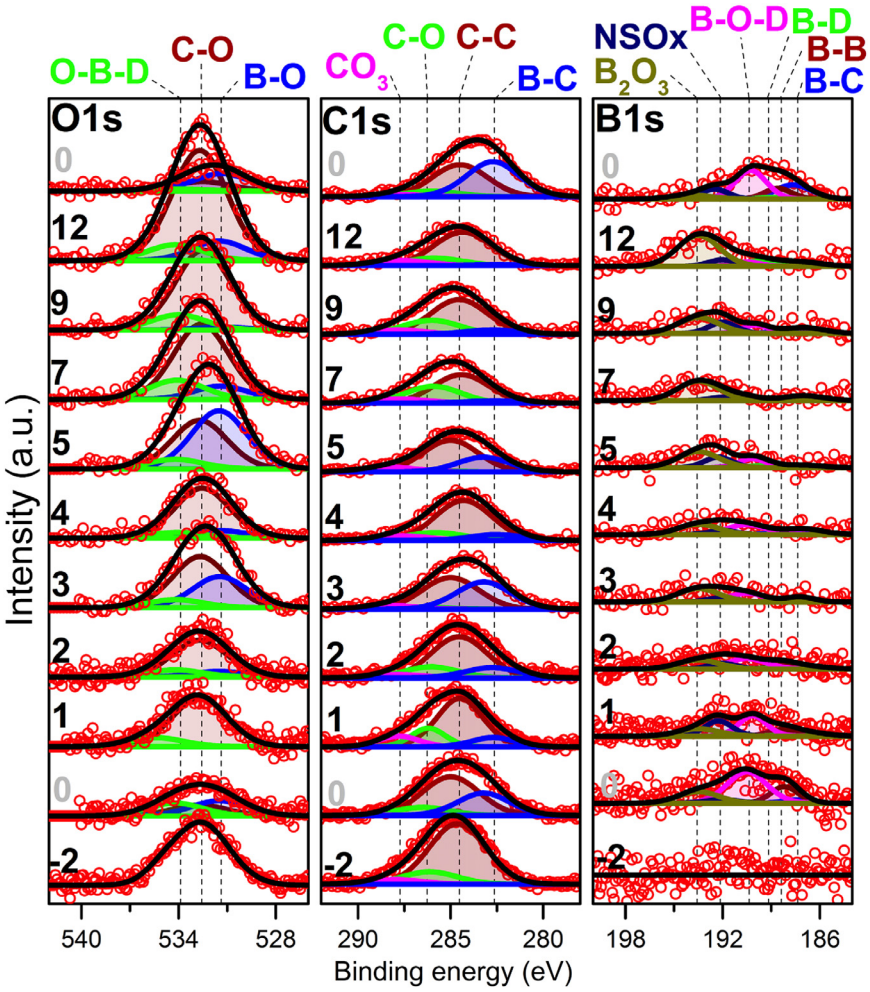

Fig. 2. O1s, C1s and B1s XPS region scans of the ATJ graphite sample. The samples were exposed to D^+ plasma discharges each day between 12 days following boronization and the XPS data were collected following the plasma exposures.

region three peaks are fitted, assigned to C–C at 284.7 eV, C–O at 286.4 eV and a slightly wider peak at 288.0 eV [27] to account for the formation of organic components e.g. CO_3 [28].

For the post-boronization, post-plasma analysis B-O and O-B-D peaks at 531.5 eV and 533.9 eV respectively were added in the O1s region [20]. Similarly, the B-C peak was added in the C1s region a 282.7 eV [21]. In the same way, a series of peaks was fitted in the B1s region i.e. B-C, B-B, B-D, B-OD and B_2O_3 at 187.2 eV, 188.1 eV, 189.1 eV, 190.2 eV, and 193.2 eV respectively. An additional peak labeled NSOx that gathers the non-stoichiometric oxides was assigned at 191.7 eV [21]. More details on the XPS data fitting can be found un Ref [29].

Fig. 2 shows the day-to-day evolution of the sample surface over the same period of twelve days. A smooth evolution of the surface chemistry is illustrated by the progressive change in the relative area of the peaks of each component in the XPS regions as it will be thoroughly discussed in Section 2.

Fig. 3 displays XPS spectra collected during a period of thirteen days with no exposure to plasma discharges. During this time the PFCs (and samples) were exposed to an Ar vent of the whole NSTX-U vessel (between days 8 and 9) and a series of Helium Glow Discharge Cleaning (HeGDC) (days 9 to 13).

4. Discussion

4.1. Chemical composition of PFCs following boronization

Fig. 1 clearly shows the appearance of the B1s XPS peak after the boronization procedure. Previous studies have compared B1s XPS spectra in samples boronized in tokamaks with reference B_4C samples [17,30]. Those studies report a peak with its center at higher energies than that of the B-B (188.1 eV) or B-C (187.2 eV) environments. The post-boronized trace in Fig. 1 ("0") shows a similar appearance with a dominant peak at 190.2 eV labeled B-O-D. The same peak can be observed in the traces labeled with "0" in Fig. 2. Hollenstein et al. [17] used the separation in binding energy between the B1s and C1s peaks as a parameter to characterize the chemical nature of post-boronization coatings in Tokamak Chauffage Alfvén (TCA). According to ref. [17] this difference is 94.5 eV for a B_4C coating compared to 96.4 eV for the pure metallic peak of B and pure graphitic state of C. The difference between the most dominant peaks in the traces labeled with 0 in Figs. 1–3 i.e. between peaks B-O-D and C–C is 94.0 eV, 94.42 eV and 93.1 eV respectively. As a consequence, our results indicate the formation of a B_4C phase during boronization in NSTX-U.

4.2. Effect of D^+ plasmas exposure on b-ATJ PFC

Following the boron deposition and with increasing D^+ fluence during plasma operations, the envelope in the B1s region in Fig. 2 shifts towards higher energies. This is a consequence of the decrease in intensity of the previously dominant B-O-D peak and an increase in area of the B_2O_3 peak, revealing an oxidation of the coatings.

The C1s region in Fig. 2 also shows important changes with boronization and plasma exposures. A low energy peak associated

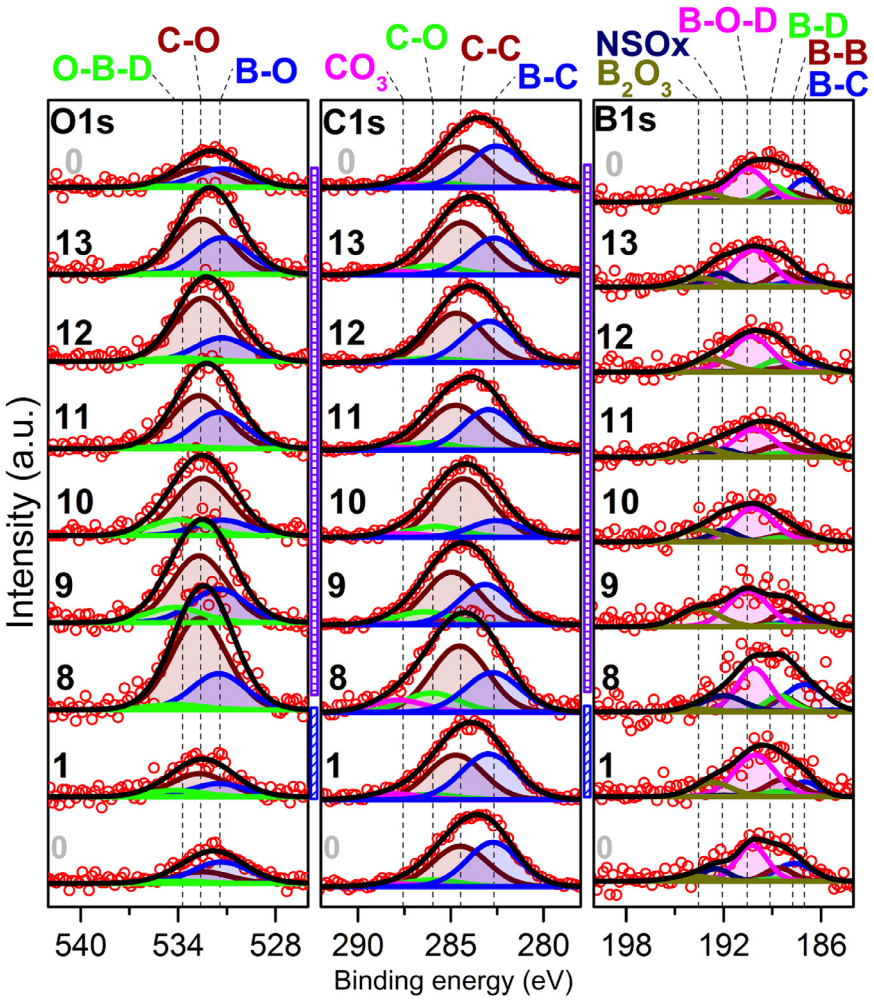

Fig. 3. O1s, C1s and B1s XPS region scans of the ATJ graphite sample. There were no D^+ plasma exposures during this span of time, an argon vent was performed between days 1 and 8 (diagonally hatched bar) and the samples were exposed to He-GDC between days 8 and 13 (horizontally hatched bar).

with B-C appears after boronization (traces "1" in Figs. 1–3). The intensity of this peak decreases with plasma exposures while the C–C peak area increases and there is a small increment in the area of the C–O peak. The oxidation phenomenon seen in the B1s region can also be seen in the O1s region, there, the B-O and C–O peaks increase with plasma operations by 40% and 25% (between "0" and "12") respectively.

4.3. Effect of residual gases, Ar exposure and HeGDC on b-ATJ

The evolution described above can be compared with that shown in Fig. 3. There, the sample was not exposed to D^+ plasmas during the depicted period, instead it only interacted with the residual gasses in the NSTX-U vessel and Ar during a maintenance vent between days 1 and 8. The changes between the traces in all regions in Fig. 3 are smaller than those seen in Fig. 1. The B-O-D peak, dominant in the B1s region after boronization, remains as the biggest contributor to the total area of the envelope during the whole period. As in the case depicted in Fig. 1 the formation of oxides is observed in Fig. 3. After the Ar vent an important change is observed in the O1s region as the C–O and B-O peaks on the traces labeled with "1" are nearly 3 and 6 times respectively larger than their counterparts labeled with 8. Although this change is not conspicuous in the B1s region, Fig. 4 shows how the oxide formation during the maintenance week is different from that formed during plasma operations. In the former oxygen reacts with boron to form mostly non-stoichiometric oxides whereas in the latter it forms B_2O_3.

The traces on Fig. 3 with labels "9" to "13" were collected following daily HeGDC (Helium Glow Discharge Cleaning) procedures. The C1s and O1s region spectra on these days are quite revealing of the surface chemistry. The O1s region shows a sudden decrease in the B-O intensity following the first He-GDC (trace 9), at the same time, the C–O signal becomes more dominant. However, the initial ratio between these peaks changes as the B-O peak grows while the C–O decreases with additional He-GDC, this trend can be clearly seen in the panel O1s of Fig. 4 (filled symbols). An analogous behavior can be seen in the C1s region in Fig. 3, there, the relative area of the B-C peak increases with respect to the C–O peak as more He-GDC is applied to the sample. This trend can be easily seen in the C1s panel in Fig. 4, there these two components (B-C and C–O) reach similar values around nine days after boronization to later diverge; with C–O decreasing and B-C increasing as days progress. The decrease in oxidized states and increase in B-C state reveals the erosion of oxides due to the He-GDC.

4.4. Comparison of the evolution of the chemical environments

Fig. 4 shows the fraction of the total XPS envelope of the fitted peaks as a function of days in for plasma exposed and non-exposed samples. The empty data points were obtained by averaging the fractions obtained during 3 different periods of boronization and

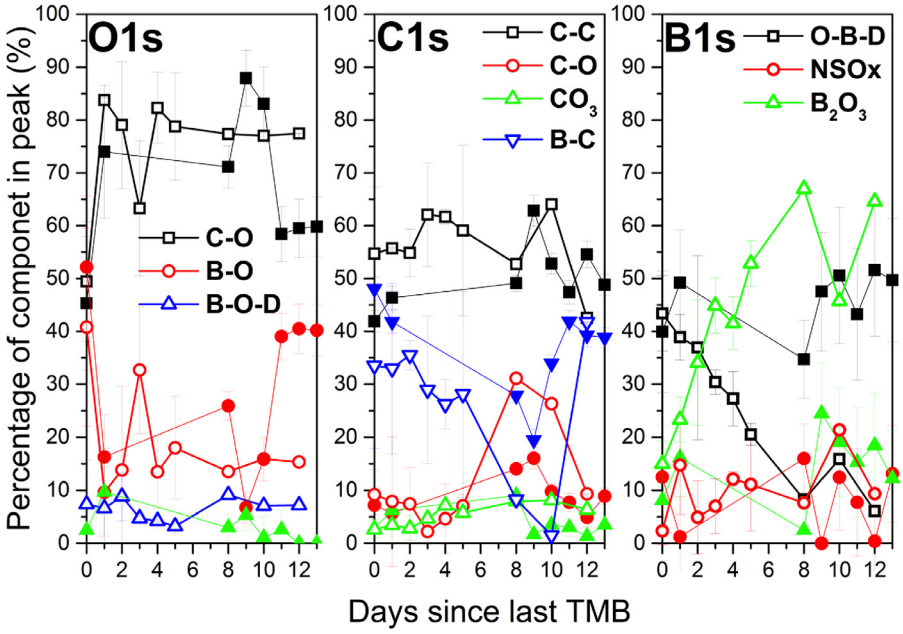

Fig. 4. Percentage of each component per region for the O1s, C1s and B1s scans as a function of the days elapsed after boronization. The filled data points show the average of percentages over three boronizations (the error bars are the standard deviation). The empty symbols show the fractions obtained with no plasma exposure. In the B1s panel only three of a total of six fitted peaks have been included for clarity.

plasma exposure. The filled points show the fractions obtained with no plasma exposure and following HeGDC. The O1s region shows an increase of the C–O fraction with a corresponding decrease in the B-O fraction, at the same time the C1s region shows the decrease in the B-C fraction and increments in the C–O component, and an early increase in the C–C fraction, followed by a steady state value. Finally, in the B1s region, the fraction of B_2O_3 increases with a marked decrease of the B-OD component. This further illustrates the descriptions provided for Figs. 2 and 3. The error bars in the plot show the standard deviation of the data sets. The small value of the variation shows that the boronizations are clearly reproducible. The XPS spectra in the three different periods studied share common features i.e. initial and final chemical composition and similar history, which in turn implies that the PFCs condition can be reset as needed with the use of boronizations.

5. Conclusions

For the first time the chemical evolution of PFCs in NSTX-U after boronization has been measured on a day-to-day basis. These measurements are among the first of their kind. Boron deposition was observed, and analysis of the separation in binding energy between the B1s and C1s peaks showed that the coatings are mostly in the form of B_4C [17]. The XPS data shows that the coatings progressively oxidize and are eroded by the increasing D^+ fluence. Oxidation was also measured during a maintenance week in which the samples did not have any plasma exposure but were exposed to an Ar vent with trace atmospheric gases. XPS data indicated that trace atmospheric oxygen reacted to form non-stoichiometric oxides instead of B_2O_3, as was the case with plasma exposure. During the maintenance period the samples were exposed to helium glow discharge cleaning, this produced an increase in the intensity of the B-C and B-O signals in the C1s and O1s region scans respectively, illustrating the cleaning effect of the glow. The initial composition and chemical state of the samples was the same after a fresh boronization, implying that the procedure yields replicable surface conditions. The data shown in this work show an improvement of at least ten in time resolution (PFC diagnosis per plasma shot) when compared with previous surface characterization studies in tokamaks. MAPP's approach of *in-vacuo* characterization of surfaces in tokamaks has been further advanced and it has provided valuable insights about the PFC chemistry/plasma performance relation

Acknowledgments

This work was supported by the US DOE contracts DE-AC02-09CH11466, DE-SC0010717 and DE-AC52-07NA27344. Additional support for F. Bedoya was provided by COLCIENCIAS via the Francisco Jose de Caldas fellowship program. The authors thank the whole NSTX team for their technical assistance.

References

[1] J. Winter, Plasma Phys. Control. Fusion. 38 (1996) 1503.
[2] J. Menard, Overview of first operational and physics results from NSTX upgrade, Nucl. Fusion (2017) in press.
[3] H.W. Kugel, et al., J. Nucl. Mater. 290 (2001) 1185–1189.
[4] H. Kugel, et al., J. Nucl. Mater. 390 (2009) 1000–1004.
[5] C.N. Taylor, et al., Rev. Sci. Instrum. 83 (2012) 10D703.
[6] H.F. Dylla, et al., J. Nucl. Mater. 63 (1976) 487–494.
[7] S.A. Cohen, et al., J. Nucl. Mater. 76 (1978) 459–471.
[8] M. Behnke, et al., Vacuum 37 (1987) 145–147.
[9] Z.S. Hartwig, et al., Rev. Sci. Instrum. 84 (2013) 123503.
[10] M. Lucia, et al., J. Nucl. Mater. 463 (2015) 907–910.
[11] O. Buzhinskij, Y. Semenets, Fusion Technol. 32 (1997) 1–13.
[12] J. Winter, et al., J. Nucl. Mater. 162 (1989) 713–723.
[13] M.M. Ennaceur, et al., J. Nucl. Mater. 280 (2000) 33–38.
[14] L.M. Litz, et al., J. Electrochem. Soc. 110 (1963) 921–925.
[15] J. Yagyu, et al., J. Nucl. Mater. 241–243 (1997) 579–584.
[16] J. Von Seggern, et al., J. Nucl. Mater. (1990) 176–177.
[17] C. Hollenstein, et al., J. Nucl. Mater. 176 (1990) 343–349.
[18] The ASDEX Team, et al., Nucl. Mater. 176–177 (1990) 350–356.
[19] Y. Nobuta, et al., Fusion Eng. Des. 81 (2006) 187–192.
[20] G.L. Jackson, et al., J. Nucl. Mater. 196–198 (1992) 236–240.
[21] F. Ghezzi, et al., Appl. Surf. Sci. 354 (2015) 408–419.
[22] Gauthier, et al., J. Nucl. Mater. 196–198 (1992) 637–641.
[23] L. Dudek, et al., Fusion Eng. Des. 87 (2012) 1515–1518.
[24] C.H. Skinner, et al., Nucl. Mater. Energy (2017) in press.
[25] H.W. Kugel, et al., J. Nucl. Mater. 313–316 (2003) 187–193.
[26] F. Bedoya, Study of Temperature Dependence of Hydrogen Retention in Lithium Coatings on Stainless Steel with the Materials Analysis Particle Probe (MAPP), MSc, University of Illinois at Urbana-Champaign, 2015.
[27] C.N. Taylor, Fundamental Mechanisms of Deuterium Retention in Lithiated Graphite Plasma Facing Surfaces, Purdue University, 2012 Doctoral.
[28] M. Phaner-Goutorbe, et al., Microsc. Microanal. Microstruct. 5 (1994) 283–290.
[29] F. Bedoya, et al., Rev. Sci. Instrum. 87 (2016) 11D403.
[30] R. Zehringer, et al., J. Nucl. Mater. 176 (1990) 370–374.